Master's thesis

NTNU
Norwegian University of Science and Technology
Faculty of Medicine and Health Sciences
Department of Clinical and Molecular Medicine

Vincent Alexander Jongen

In vitro effects of radiation and mechanical load on murine osteocytes MLO-Y4

Master's thesis in Molecular Medicine
Supervisor: Astrid Kamilla Stunes
May 2020

NTNU
Kunnskap for en bedre verden

Vincent Alexander Jongen

In vitro **effects of radiation and mechanical load on murine osteocytes MLO-Y4**

Master's thesis in Molecular Medicine
Supervisor: Astrid Kamilla Stunes
May 2020

Norwegian University of Science and Technology
Faculty of Medicine and Health Sciences
Department of Clinical and Molecular Medicine

NTNU
Norwegian University of
Science and Technology

Table of Content

1. Acknowledgements

The work in this thesis was performed at the Department of Clinical and Molecular Medicine, Faculty of Medicine and Health sciences, Norwegian University of Science and Technology (NTNU) Trondheim, Norway in the academic year 2019-2020.

Along the road to complete this thesis I was supported by many wonderful people without whom I would have never been able to make it this far. I would like to take this opportunity to express my thanks to everyone that has met and supported me along the way.
I would especially like to show my gratitude to these people in particular:

My supervisor Astrid Kamilla Stunes who introduced me to the field of bone biology. Her guidance and advice were of tremendous value to overcome the various obstacles that came up along the way. Her door was always open for questions or just friendly conversation. My co-supervisor Mats Peder Mosti I would like to thank for his good advice and fruitful discussion. His input was most certainly appreciated.

I would like to give my special thanks to Kathrine Røe Redalen and Anne Beate Langeland Marthinsen, who were more than willing to assist in the radiation experiments that form the basis of this work. Without their generosity and expertise, none of this had been possible.

My fellow master students Mathilde Skistad Homstad and Md Abu Jafar Sujan, with whom I spent many hours in the lab. They shared with me the many accomplishments and set-backs that come with cellular and molecular research.

And last but not least, my friends and family. Most notably my parents and sister, Marianne Vinken, Jo Jongen, and Lynn Jongen, who were always there for me. My flatmates, Adelle Basson, Joshua Baskaran, and Klara Krpina, who were like a new family when my old family was so far away, and my girlfriend Romana Malečková, who was always with me from a distance. Without you all I would not have been able to complete this challenge.

2. Abbreviations

CTIBL	Cancer treatment induced bone loss
HSC	Hematopoietic stem cell
MPP	multipotent progenitor
CMP	Common myeloid progenitor
M-CSF	Macrophage colony stimulating factor
RANK	receptor activator of NF-κB
OPG	osteoprotegerin
MMP	matrix metallopeptidase
MSC	mesenchymal stem cells
Runx2	runt-related transcription factor 2
SOST	sclerostin
DKK1	Dickkopf-related protein 1
Dlx5	distal-less homeobox 5
Osx	osterix
ALP	Alkaline phosphatase
BSP	Bone sialoprotein
OCN	osteocalcin
PGE_2	Prostaglandin E_2
BLC	Bone lining cells
FBS	Fetal bovine serum
CS	Calf serum
HRP	Horse radish peroxidase
AChE	Acetylcholine esterase
MTT	3-(4,5-dimethylthiazol-2-yl)-2,5-diphenyltetrazolium bromide
LDH	lactate dehydrogenase

3. Summary

The increased survival rates for cancer as a result of improved diagnosis and treatment has come with the drawback that cancer treatment side effects are becoming more frequent as well. Cancer treatment induced bone loss can be caused by a variety of different treatment regimes, one of these being radiotherapy. Previously most research on the effects of radiation on bone tissue has focussed on the bone synthesizing osteoblasts and the bone resorbing osteoclasts. In the first part of this study, the effects of radiation on osteocyte survival and gene expression is investigated using the MLO-Y4 osteocyte cell line.

A growing body of evidence shows that mechanical loading of the bones has a positive effect on bone health and bone strength. It is therefore hypothesised that mechanical loading could play a role in the prevention of radiation induced bone loss. In the second part of this study, the combined effect of radiation and mechanical load on osteocyte survival and gene expression has been investigated using a fluid flow shear stress system to mimic mechanical loading of the osteocytes. It was shown that a radiation dose of 5 Gy induces apoptosis within 24 to 48 hours and increased RANKL expression. Fluid flow shear stress was shown to decrease apoptosis following radiation and decrease the RANKL:OPG gene expression while increasing Bcl2:Bax gene expression. Taken together, these findings seem to support the hypothesis that mechanical loading of bones may help in the protection against radiation induced bone loss, by reducing osteocyte apoptosis.

4. Introduction

The ever growing knowledge on the biology of cancer has led to improved diagnostic and therapeutic treatments, thereby improving overall survival rates. Regrettably, these increasingly long treatments often lead to a wide variety of side effects. These side effects can range from disturbed sleep and fatigue to neuropathy or immune related adverse effects. (1-3) Additionally, anti-tumour therapies are often associated with cancer treatment induced bone loss (CTIBL). Hormone therapies, chemotherapies, tyrosine kinase inhibitors (TKIs) and radiotherapy are all linked to CTIBL. (4-6)

4.1 Bone biology and bone cells

Despite the bones inert appearance as a mineralized connective tissue, bone fulfils a wide variety of important functions. These functions include the support and protection of softer organs and tissues, enabling locomotion, storing calcium and phosphate and sheltering bone marrow. (7) In addition to its mineralized extracellular matrix, bone consists of four main cell types. These four cell types, osteoblasts, osteoclasts, osteocytes and bone lining cells, are all working together to maintain a balance between bone resorption and bone formation. The osteoblasts produce the bone matrix whereas the osteoclasts break it down. Osteocytes regulate the function of osteoblasts and osteoclasts. The exact function of bone lining cells is poorly understood, although they do seem to play a role in the regulation of osteoblast and osteoclast activity as well as preventing direct contact between osteoclasts and the bone matrix. The process of bone resorption and subsequent formation is called bone remodelling. Bone remodelling takes place to maintain bone strength through the renewal of microdamaged bone, but it also contributes to maintaining mineral homeostasis. Additionally, by shifting the balance between bone formation and bone resorption, bone remodelling allows the bone to adapt to environmental cues such as mechanical stress or prolonged unloading. (8) A dysregulation of the bone remodelling process may lead to the development osteoporosis, which is caused by a higher bone resorption than bone formation. (9)

4.1.1.1 Osteoclasts

The osteoclast is the only cell type of the four main types of bone cells that is derived from hematopoietic stem cells instead of mesenchymal stem cells. (10) Osteoclasts are responsible for bone resorption and set themselves apart from the other bone tissue cell types with their highly segregated membrane domains. In addition, osteoclasts exhibit a very characteristic

organelle distribution. Osteoclasts are large multinucleated cells. The large volume of these cells allows them to cover a larger surface area of the bone, thereby increasing the efficiency of bone resorption. Vacuoles, lysosomes and mitochondria are numerous and mostly located at the side of the cell adjacent to the mineralized bone. (9, 11)

Osteoclasts differentiate from hematopoietic stem cells (HSC) through a stepwise process. Initially, HSCs become multipotent progenitors (MPP), losing the capability for self-renewal. Multipotent progenitors are able to differentiate further into a variety of cell types, one of which is the common myeloid progenitor (CMP) that can eventually give rise to the osteoclast progenitor cells. Stimulation of osteoclast progenitor cells will lead to the generation of mature osteoclasts. (10)

Osteoclast precursor formation takes place in the bone marrow, through the expression of macrophage colony stimulating factor (M-CSF) receptors, marking the transition of MPP to CMP. Binding of M-CSF to the M-CSF receptors on the CMP surface induces expression of receptor activator of NF-κB (RANK), which functions as the receptor for RANK ligand (RANKL). RANK expression is a major step in the differentiation of CMP into osteoclast progenitors. The progenitor cells migrate to the bloodstream where they remain until the osteoclast progenitors are eventually attracted to the bone tissue again by the presence of M-CSF and RANKL in remodelling bone. (12)

4.1.1.2 RANK/RANKL/OPG

Osteoclast maturation and activation in bone tissue is stimulated by the association of RANKL and its receptor, RANK. RANKL is mostly expressed by osteoblasts, osteocytes and stromal cells, but also B and T cells can be a source of RANKL. (9, 12) RANKL is generally found as a membrane-bound molecule, with the excreted form being the result of proteolytic cleavage by matrix metallopeptidases (MMPs). Both the membrane-bound and excreted forms of RANKL have an osteoclastogenic effect. (10, 13) The RANK-RANKL interaction can be further attenuated by competitive binding of RANKL to osteoprotegerin (OPG), preventing RANKL from binding the RANK receptors on the osteoclasts. It is important to note that, despite both being from the TNFR superfamily, OPG has a higher affinity for RANKL than RANK has, due to OPGs ability to rotate more than RANK. (10) OPG is mainly expressed by osteoblasts and osteocytes as a result of canonical Wnt/β-catenin signalling. (9) Osteoclastogenesis is therefore regulated by the dynamic balance between RANKL/OPG expression of osteoblasts and osteocytes in remodelling bone tissue. (9, 10, 12, 13) The

RANKL cytokine is encoded for by *Tnfsf11*, whereas receptor RANK and decoy receptor OPG are encoded by *Tnfrsf11a* and *Tnfrsf11b* respectively. (10)

4.1.1.3 Osteoclast membrane domains

When the multinucleated osteoclasts are in direct contact with the mineralized bone matrix, four distinct membrane domains form. (9) The apical membrane faces the bone matrix and consists of a ruffled border and sealing membranes. The ruffled border is a cluster of membrane extensions, comparable to microvilli. The sealing membranes contain no cell organelles but many podosomes, which are adhesional structures that enable strong and dynamic attachment to the bone matrix. (11, 14) The basolateral and functional secretory domains of the osteoclast membrane are not in direct contact with the mineralized bone matrix but face the vasculature. (9)

4.1.1.4 Bone resorption

Within the cytosol of activated osteoclasts, carbonic anhydrase type 2 (CA2) facilitates the conversion of carbonic acid into H^+ and HCO_3^-. To prevent alkalinisation of the cytosol, HCO_3^- is transported out of the cell in exchange for Cl^- by the anion exchanger SLC4A2. H^+ is excreted into the resorption lacuna, also called Howship lacuna, by V-ATPases. The acidification of the resorption lacuna allows for the dissolution of the inorganic compounds of the bone matrix. Cl^- is transported to the resorption lacuna by ClC7, a $2Cl^-/1H^+$ antiporter, to neutralize the positive charge. Degradation of the organic components of the bone matrix, mostly collagen type 1, is facilitated by a variety of excreted lysosomal enzymes. The acidic environment of the resorption lacuna activates the cysteine proteinase cathepsin K and tartrate resistant acid phosphatase (TRAcP). Osteoclasts also express various matrix metalloproteinases (MMP), most notably MMP9, which further assist in the degradation of collagen type 1. (9-11)

It is interesting to note that the ions and enzymes that play a role in bone resorption are mostly excreted on the outer regions of the ruffled border, forming the fusion zone, whereas the degraded matrix components are transcytosed through the uptake zone and functional secretory domain in the inner regions of the cell. (11)

4.1.2.1 Osteoblasts

Unlike osteoclasts, osteoblasts are derived from the pluripotent mesenchymal stem cells (MSC), just like adipocytes or chondrocytes. (15) About 4% to 6% of the bone cells are made

up of osteoblasts, whose main function it is to synthesise the mineralized bone matrix that give bone tissue its rigid structure. (9, 16) More recently, osteoblasts have been found to also exhibit endocrine functions, influencing insulin production and sensitivity as well as neurotransmitter production. (17) Additionally, aging osteoblasts have the ability to differentiate further into bone lining cells or osteocytes. (9, 16) Osteoblasts are polarised cells that secrete their osteoid towards the growing bone matrix. As expected the osteoblasts share the morphological features of many other protein synthesising cells. Osteoblasts have large amounts of rough endoplasmic reticulum and an elaborate Golgi apparatus. Additionally, osteoblasts contain a variety of secretory vesicles. (9)

The initial commitment of MSC towards the osteoprogenitor lineage requires a variety of pro-osteogenic pathways (Figure 1). Chiefly among these are Wnt and bone morphogenetic (BMP) regulated pathways, which drive osteoblast differentiation and increase the expression of runt-related transcription factor 2 (Runx2). (7, 9, 16) The canonical Wnt-signalling pathway can be further attenuated by the antagonists sclerostin (SOST) and dickkopf-related protein 1 (DKK1) produced by osteocytes. Expression of Runx2, Distal-less homeobox 5 (Dlx5) and Osterix (Osx) is required for the differentiation of MSC into osteoblast progenitors, the first step towards osteoblasts. (9, 15, 16) Knock-out experiments have shown that Runx2 is a master gene in the development of osteoblasts as Runx2-null mice completely lack osteoblasts. (18) Runx2 has been shown to upregulate many osteoblast-related genes, including ColIA1, Alkaline phosphatase (ALP), bone sialoprotein (BSP) and osteocalcin (OCN). Expression of ALP characterises the development of osteoblast progenitors into pre-osteoblasts. The pre-osteoblasts go through a proliferation phase before maturation into osteoblasts. Mature osteoblasts show increased expression of Osx, OCN, BSP1, BSP2 and collagen type 1. (9, 15, 16)

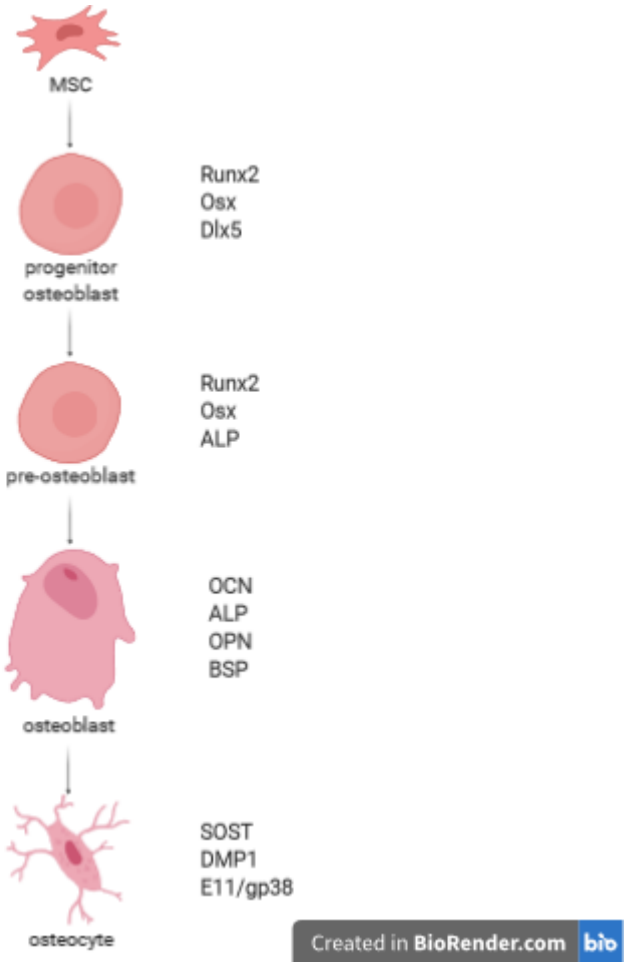

Figure 1: Differentiation of mesenchymal stem cells into osteoblasts and osteocytes.
Schematic figure of the stages of osteoblast and osteocyte development and their relevant differentiation markers. Figure was created using BioRender.com.

4.1.2.2 Bone synthesis

The process of bone matrix synthesis takes place in two steps. The first step is the deposition of the organic matrix, called the osteoid, and the subsequent step is the mineralization of the osteoid. The secreted osteoid mainly consists of collagen type 1, but also non-collagen proteins (such as OCN, osteonectin, BSP 2 and osteopontin) and proteoglycans (such as decorin and biglycan). The mineralization of the osteoid also takes place in two phases, the vesicular and the fibrillar phase. The vesicular phase takes place in vesicles, called matrix vesicles, secreted by the osteoblasts. A variety of proteins allow for the uptake of calcium and phosphate into the matrix vesicles. Once the concentration of calcium and phosphate exceeds the maximum concentration of solubility, tricalcium phosphate crystals will form. Hydroxylation of these crystals will lead to the formation of hydroxyapatite, $Ca_{10}(PO_4)_6(OH)_2$. Supersaturation of phosphate and calcium ions within the matrix vesicles

will eventually lead to rupture of the vesicles, starting the fibrillar phase. During the fibrillar phase, the hydroxyapatite crystals fill the gaps in the bone matrix. (9, 16)

4.1.3.1 Osteocytes

By far the most abundant cells in the bone are the osteocytes, which make up 90-95% of all cells in the bone. Osteocytes are characterised by their dendritic morphology. Osteocyte descend from osteoblasts and are the most long-living cells found in the bone, with a lifespan of up to 25 years. (16) The osteocytes can be found embedded in the mineralized bone matrix and were therefore initially difficult to isolate and study. The development of new techniques led to the discovery that, contrary to previous assumptions, osteocytes perform numerous important functions in bone. (9, 19) The cell bodies of the osteocytes are located in lacunae within the bone matrix. Small channels, called canaliculi, radiate outwards from the lacunae, allowing the cytoplasmic processes of the osteocytes to connect to neighbouring osteocytes and osteoblasts. Gap junctions between the osteocyte and its neighbouring cells allow for intercellular communication. (20) Osteocyte gap junctions are mainly composed by connexin43, the main connexin in bone tissue. The network of lacunae and canaliculi is called the lacunocanalicular system. The lacunocanalicular system is filled with an extracellular fluid, which allows for cell-cell communication and plays a key role in the mechanosensing abilities of osteocytes. (9) Osteocytes are seen as the main regulators of bone remodelling through their regulation of osteoclasts and osteoblasts. (9, 19, 20)

As mentioned, osteocytes differentiate from osteoblasts (Figure 1). During differentiation, the rounded osteoblasts become encased in osteoid. Processes start to form as the cell body decreases in size. Additionally, the number of cell organelles decreases and as the osteoid mineralizes, the endoplasmic reticulum and Golgi apparatus decrease. (16) As the osteoblasts develop into osteocytes, the expression of ALP, OCN and BSP2 decrease. (16, 19) The metalloproteinase MT1-MMP is a membrane-anchored proteinase that cleaves collagen and other matrix molecules to allow for the formation of the canaliculi. At the same time, osteocytes start to express E11/gp38, which plays a role in the extension of the dendrites. (19) As the osteoid surrounding the osteocytes mineralizes, expression of osteocyte markers, such as sclerostin and dentine matrix protein 1 (DMP1), increase. (16, 19)

4.1.3.2 Mechanosensation by osteocytes

Bone has long been known to respond to mechanical cues. Increased loading, as is the case with exercise, increases bone mineral density and bone mass, whereas decreased loading, as is

the case in bedrest or microgravity, leads to decreased bone mass and mineral density. It was proposed that mechanical loading led to fluid flow within the lacunocanalicular system, but the underlying mechanism to turn this mechanical cue into a biological system remained a mystery. (21) The piezoelectric effect is the translation of mechanical stimulations into biochemical signals. Osteocyte shape and location contribute to this mechanosensitive function. (9)

It was first proposed in 1977 that mechanical load of bones leads to small deformations that lead to fluid flow. This was initially thought to be the mechanism for nutrient supply to the osteocytes embedded within the mineralized bone matrix. (22) Almost 20 years later it was proposed that this fluid flow took place in the lacunar-canalicular system and that it caused a strain generated potential within the bone cells. Mathematical models predicted that the fluid shear stress on the osteocytes was comparable to that on vascular endothelium cells in capillaries, about 8 to 30 dynes/cm^2 . (23, 24) The processes of osteocytes are suspended within the canaliculi by tethers. Fluid flow through the canaliculi creates a tension on these tethers, amplifying the strain by a factor of 10 to 100. (25)

Santos et al. established that mechanical loading of MLO-Y4 osteocytes activated the β-catenin signalling pathway via a mechanism involving nitric oxide, focal adhesion kinase and the Akt signalling pathway. (26) More recently, Li et al. reported that induction of the ion channel protein Piezo1 by fluid flow as a model of mechanical stimuli increased Wnt1 expression in osteocytes through the activation of YAP1 and TAZ. (27) Wnt1 is an inducer of osteoblastogenesis, mostly derived from osteocytes. (28) This suggests that Piezo1 is a mechanosensitive ion channel that plays a fundamental role in the response of osteocytes to mechanical load. (27)

Osteocytes display a wide variety of effects in response to fluid flow. Fluid flow causes a rapid increase in nitric oxide, PGE_2, PGI_2 and Wnt1 expression. Moreover, fluid shear stress has been demonstrated to inhibit osteocyte apoptosis and osteoclastogenesis whereas unloading leads to increased hypoxic and apoptotic osteocytes. (21, 29, 30) Lastly, mechanical load seems to lead to the better healing of the bone after fracture. (29)

4.1.3.3 Osteocytes as regulators of osteoclast and osteoblast activity

One of the main functions of osteocytes is the regulation of osteoblast and osteoclast activity. Bone remodelling by osteoclasts and osteoblasts replaces microdamaged bone. At the sites of microdamage, osteocyte apoptosis occurs. The apoptotic bodies of the osteocytes express

RANKL to recruit osteoclasts. (19, 20) Additional apoptotic products of osteocytes include vascular endothelial growth factor (VEGF), ATP, sphingosine-1-phosphate, and other chemokines to attract bone cell precursors. (20) Also in the absence of microdamaged bone, osteocytes play a key role in the regulation of bone remodelling in response to either hormonal or mechanical cues. (9, 16, 20) Mechanically loaded osteocytes release PGE_2, which activates β-catenin signalling in osteocytes to prevent apoptosis. This response is further enhanced by major gap junction protein connexin43, which allows for communication between osteocytes. (31, 32) Moreover, following an increase in mechanical load, osteocytes increase the expression of Wnt1 and decrease the expression of DKK1 and sclerostin, thereby increasing Wnt-signalling in osteoblasts. (20, 27) Additionally, parathyroid hormone (PTH) has the ability to decrease osteocyte expression of sclerostin. (16, 20) In contrast, mechanical unloading leads to an increase in osteocyte expression of RANKL, thereby stimulating osteoclastogenesis. (20) In addition to RANKL, osteocytes are also a major source of OPG. Osteocytes are therefore able to shift the RANKL/OPG balance to either increase or decrease osteoclastogenesis in response to environmental cues. (9, 16, 20)

4.1.4 Bone lining cells

Bone lining cells (BLCs) are quiescent osteoblasts that reside on the surface of the mineralized bone. The BLCs are connected to adjacent BLCs and osteocytes via gap junctions. These cells are flat shaped and contain very few cellular organelles, due to their low metabolic activity. The exact function of bone lining cells is poorly understood but BLCs prevent osteoclasts from breaking down bone matrix when resorption is not needed. (9, 33) BLCs have the ability to develop into mature osteoblasts. Additionally, BLCs can influence osteoclastogenesis through the expression of OPG and RANKL. (34)

4.1.5. Extracellular matrix

The vasculature and the four cell types mentioned above make up less than 10% of the volume of bone, whereas the extracellular matrix makes up the remaining 90%. About one third of the weight of the extracellular matrix comprises of organic matrix, with the remaining two thirds comprising of the inorganic fraction. The organic matrix is made up mostly of crosslinked collagen type 1, but also contains non-collagenous proteins and proteoglycans. The organic matrix is what gives bone its yield strength or toughness. (33) The inorganic fraction of the bone matrix is chiefly made up of hydroxyapatite, but also contains bicarbonate, sodium, potassium, citrate, magnesium, carbonate, fluorite, zinc, barium, and

strontium. (9) It is estimated that 99% of the calcium, 85% of the phosphate and 50% of the sodium and magnesium of the entire body are stored within the bone matrix. It is this inorganic fraction that gives bones their tensile strength. (33) Osteoblasts and osteoclasts bind the RGD sequences of bone matrix proteins such as osteopontin. Osteocyte processes, which are located in the canaliculi, are in contact with the bone matrix via tethers or bind the matrix directly at the hillocks, which are structures protruding from the canalicular walls. (9)

4.1.7 Bone remodelling and the basic multicellular unit

When bone remodelling is required, a structure called the basic multicellular unit forms. This structure contains a cutting cone of osteoclasts at the front and a closing cone of osteoblasts at the back. The unit is covered by bone lining cells. (9, 13, 35) The bone remodelling process takes place in three stages. During the first step, osteoclasts resorb the bone matrix. The second step is a transitional step during which both bone resorption and bone synthesis takes place. In the final step, osteoblasts synthesise the bone matrix. Both the bone lining cells and the osteocytes play a role in the regulation of these three phases. (9, 35) The bone remodelling is initiated by the attraction of osteoclasts by RANKL and M-CSF. During the resorption phase, osteoblasts are suppressed by semaphorin4D (sema4D), which is expressed by the osteoclasts. (36) Another semaphormin, sema3A, is expressed by osteoblasts to inhibit osteoclast differentiation. (37, 38) An additional coupling mechanism involves the interaction of ephrinB2 and ephrinB4. When ephrinB2, expressed by osteoclasts, interacts with ephrinB4, expressed by osteoblasts, it leads to the suppression of the osteoclast differentiation and the stimulation of the osteoblast differentiation. EphrinB2/EphrinB4 signalling therefore contributes to the shift from bone resorption to bone formation. (39) Additional regulation of the bone remodelling process is mediated by osteocytes, which are a major source of regulating factors of both osteoblast and osteoclast activity. Moreover, osteocyte apoptosis has been found to act as a chemotactic signal leading to osteoclast recruitment. (9)

4.2 Cancer treatment induced bone loss (CTIBL)

The bone turnover to maintain bone health is a tightly regulated process. Many cancer treatments influence the regulation of bone turnover, and may lead to the development of bone loss and osteoporosis. Additionally, both cancer and its treatment lead to deterioration of both the mental and physical condition of the patient. This often results in a decreased physical activity, which has been shown to be a contributing factor in osteoporosis.

Subsequently, osteoporotic bone creates a favourable environment for metastatic tumour growth, leading to a vicious downwards spiral. (5)

Estrogens and androgens both influence the regulation of bone resorption and synthesis. Both osteoblasts and osteoclasts express estrogen receptors. Activation leads to increased secretion of IGF-1, TGFβ and OPG, thereby shifting the balance in favour of bone synthesis. (40) Through the process of aromatization, testosterone can be converted into estradiol, leading to an indirect stimulation of osteoblast proliferation by testosterone. Androgens can also stimulate the differentiation and proliferation of osteoblasts directly by binding androgen receptors on the osteoblasts, although to a lesser extent than estradiol. (41, 42) Prostate cancer and estrogen receptor positive breast cancer are both commonly treated with gonadotropin releasing hormone (GnRH) agonists. (43, 44) Persistent activation of GnRH receptors will in the long term lead to a reduction of androgens and estrogens, thereby increasing bone resorption and decreasing bone formation. (5)

Another common cancer treatment is chemotherapy. Many compounds used in chemotherapy, most notably platinum compounds such as cisplatin or ifosfamide, lead to kidney impairment and electrolyte disorders. (5) Chemotherapy can also induce bone loss through ovarian failure which results in estrogen defincieny. Additionally, doxorubicin and paclitaxel have been shown to induce senescence of bone cells, leading to increased bone loss. (4)

Radiotherapy induced bone damage is caused by a variety of effects. Hypogonadism and electrolyte disorders are indirect effects of radiotherapy leading to bone loss. Radiotherapy also directly affects the bone cells, leading to an imbalance in osteoblast and osteoclast activity. (5) Irradiation induced bone loss is shown to be a result of the suppression of osteoblasts as well as the increased differentiation of osteoclasts with the mesenchymal stem cell derived cell lines appearing to be more vulnerable to radiation than the hematopoietic cell lineages. More recently, the effect of radiation on osteocytes has been explored and radiation was shown to reduce osteocyte viability and induce apoptosis, but the exact molecular mechanisms are still poorly understood. (45-47) Radiation of osteocytes has also been shown to increase SOST expression as well as the RANKL/OPG expression ratio. (45, 48)

4.3 Apoptosis

Radiotherapy induces apoptosis, which takes place through the activation of the caspase cascade. Caspases are a family of cysteine proteases. Most caspases are initially expressed as pro-caspases that can be activated by proteolytic cleavage. (49) The apoptosis pathway is

initiated when BH3 inactivates Bcl2-like proteins and repeals the inhibition of Bax and Bak, which trigger the release of cytochrome c from the mitochondria. In the cytoplasm, cytochrome c can activate apoptotic protease-activating factor 1 (Apaf-1). Apaf-1 activates the caspase cascade by activating caspase 9, which in turn activates caspases 3, 6 and 7. (50)

5. Research Problem

Radiotherapy against cancer can lead to CTIBL and osteoporosis. These conditions lead to increased fraction risk and decreased quality of life for the patients, create an environmental niche that stimulate further tumour growth and metastasis and drive up healthcare cost. (5) The effects of radiotherapy on osteocytes are still poorly understood. A better understanding of the effects of radiation on osteocytes could lead to the development of new treatments of CTIBL. The first aim of this study is therefore to investigate the effects of radiation on survival, cell viability and gene expression in osteocytes *in vitro*.

Mechanical load on bones seems to have a positive effect on bone mineral density, protects against osteoporosis and leads to better healing of fractures. Fluid shear stress on osteocytes has been shown to protect against apoptosis. (29, 30) The second aim of this study is therefore to investigate the combined effect of radiation and fluid shear stress on osteocytes *in vitro* to investigate whether mechanical load can counteract the negative effect of radiation. This is a part of an ongoing project to examine whether exercise during radiotherapy could be utilized to reduce long-term radiotherapy-induced bone loss in cancer patients.

6. Methods

6.1 Cell system

The murine long bone osteocyte Y4 (MLO-Y4) cell line, provided by Prof. Lynda F. Bonewald, University of Missouri, USA, was chosen for its sensitivity to mechanical load in the form of fluid flow. (27, 32) The MLO-Y4 cells were seeded on rat tail type 1 collagen (Becton Dickson Bioscience) coated flasks, dishes and plates. The cells were maintained using minimum essential medium alpha (MEM-α) (Invitrogen). The medium was supplemented with 1% L-glutamine (Gibco), 1% penicillin/streptomycin (Gibco), 0.4% fungizone (Gibco) and 1mM sodium pyruvate (Gibco BRL, Life Technologies Ltd, Scotland). Additionally, in the first two passages after thawing, the medium was enriched with 10% fetal bovine serum (FBS) (EuroClone, UK) and 10% calf serum (CS). In later passages the medium was enriched with 5% CS and 5% FBS. Cells were split 1:4, when reaching 60-70% confluence, by using 0.05% trypsin/0.5mM EDTA solution (Lonza). After each splitting 25-50% of the self-conditioned medium was used again in addition to 50%-75% new medium. Cells were cultured at 37°C and 5% CO_2.

6.2 Radiation

Radiation was performed by the Department for radiation therapy of St. Olav's Hospital (Trondheim, Norway). Cells were seeded two days prior to radiation. The cells were radiated with a dose of 5 Gy using a linear accelerator for photon radiation. Medium was changed to MEM-α containing 1% fetal bovine serum after radiation. Non-radiated cells were used as control.

6.3 Fluid flow system

Cells were seeded on rat tail collagen coated culture slides at 150,000 cells/slide in 3 ml MEM-α containing 5% CS/FBS two days prior to treatment. The cells were exposed to fluid flow shear stress by the Flexcell Fluid Shear System (Flexcell, USA). Fluid shear stress was gradually increased to 10 dynes/cm^2 over a period of 5 minutes. A 10 dynes/cm^2 fluid shear stress was maintained for 2 hours before gradually decreasing back to 0 dynes/cm^2 over a period of 5 minutes. All slides were taken out of the Fluid Shear System and 1.5 ml MEM-α + 1% FBS was added to the cells for incubation.

6.4.1 ELISA for cell death and PGE_2 expression - Principle

Enzyme linked immune sorbent assay (ELISA) is a commonly used biochemical method for the detection of a large variety of ligands. In this study, ELISA was used to look for an enrichment of mono- and oligonucleosomes in the cytoplasm, a marker for cell death, of radiated cells. Additionally, ELISA was used to assess the excretion of PGE_2 in response to fluid flow.

In the ELISA used to detect cell death, the bottoms of a 96 well plate were covered with anti-histone antibodies to capture the histone-bound nucleosomes. A secondary antibody that binds DNA is labelled with horse radish peroxidase (HRP). The HRP-labelled antibody binds the captured nucleosomes. The amount of bound HRP can be photometrically determined by the addition of a substrate that turns green in the presence of HRP.

For the detection of PGE_2 an acetylcholinesterase competitive ELISA was used. In this ELISA the 96 well plates contain a limited amount of PGE_2 binding antibodies. The PGE_2 containing sample is added as well as a constant amount of acetylcholinesterase-PGE_2 conjugate. The sample-derived PGE_2 and the conjugate will competitively bind the limited antibody. The amount of conjugate able to bind the antibody is inversely related to the amount of PGE_2 present in the sample. Ellman's reagent, which contains the acetylcholinesterase substrate, is added after washing away the unbound conjugate. This will lead to a reaction product with a distinct yellow colour that can be photometrically quantified.

6.4.2 ELISA for cell death and PGE_2 expression – Protocol

Cell death was assessed using Cell Death Detection Kit ELISA Plus (Roche Applied Sciences, Germany). The cells were seeded at 5000 cells/well in 100 µL MEMα and incubated at 37 °C and 5% CO_2 for 24 hours before being subjected to radiation. Cell death detection was done 24 hours and 48 hours after radiation. The medium in all wells was replaced with 200 µL lysis buffer and incubated for 30 minutes at room temperature. After centrifugation at 200g for 10 minutes, 20 µL of the supernatant was transferred to the streptavidin coated plate. 80 µL of immunoreagent was added to all wells and incubated for 2 hours on an orbital shaker (300 rpm) at room temperature. All wells were washed thrice with incubation buffer before adding 100 µL ABTS substrate. After 15 minutes on an orbital shaker (250 rpm), 100 µL stop solution was added to each well. Absorbance was measured at 405 nm using an iMark microplate absorbance reader (BioRad).

PGE_2 secretion was quantified using a Prostaglandin E_2 ELISA kit -Monoclonal from

Cayman Chemical (Ann Arbor, USA). Cells were subjected to radiation either with or without subsequent fluid flow treatment. Cultured medium was collected at 2 hours, 24 hours and 48 hours after treatment. All medium samples were diluted 1:10 in ELISA buffer. 50 µL of the diluted medium sample was added per well. 50 µL of PGE_2 AChE tracer and 50 µL of PGE_2 antibody were added to the samples and incubated for 18 hours at 4 °C. All samples were washed five times with washing buffer before addition of 200 µL Ellman's reagent. The samples were incubated for 60 minutes on an orbital shaker (200 rpm) protected from light, at room temperature. Absorbance at 415 nm was measured using an iMark microplate absorbance reader (BioRad).

6.5.1 MTT assay - Principle

To look at cell viability instead of apoptosis or cell damage, MTT assays were performed. Metabolically active cells contain NAD(P)H dependent oxidoreductase enzymes. In an MTT assay the tetrazolium salt MTT is added to the cells. The mitochondrial reductases of viable cells reduce the yellow coloured MTT to the purple coloured formazan. Since formazan will form in the shape of insoluble crystals, acidified sodium dodecyl sulfate (SDS) is added to gain a purple coloured solution. (51, 52)

6.5.2 MTT assay - Protocol

Cell viability was determined using the CellTiter 96 Non-Radioactive Cell Proliferation Assay (Promega, Madison, USA). The cells were cultured in 96 wells plates at a density of 1000 cells/well. At either 2, 24, 48, 72 and 120 hours after radiation, 20 µl dye solution was added to cells in 100 µl medium and incubated for 3 hours at 37 °C. To stop the reaction, 100 µl SDS stop solution was added to the wells. 100 µl was transferred to a new plate after 24 hour incubation at 37 °C. Absorbance was read at 570 nm using a reference wavelength between 630 and 750 nm on an iMark microplate absorbance reader (BioRad).

6.6.1 Lactate dehydrogenase assay - Principle

Cytotoxicity in the cells caused by radiation can also be measured by the presence of extracellular lactate dehydrogenase. Lactate dehydrogenase (LDH) is a stable enzyme present in the cytosol of the cells. Damage to the cells plasma membrane will lead to the release of LDH into the cell culture medium. In the presence of NAD^+, lactate is converted into pyruvate, forming NADH+ H^+ in the process. Diaphorase, a catalyst, can the transfer the H/H^+ to a tetrazolium salt to form formazan salt. This leads to an observable change in colour.

Increases in plasma membrane damage will lead to an increase in available LDH, and therefore higher levels of formazan salt. (51, 53)

6.6.2 Lactate dehydrogenase assay - Protocol

Levels of cytotoxicity were determined using the Cytotoxicity Detection Kit plus (LDH) purchased from Roche Applied Science (Germany). 100 µl of cultured medium was taken from the cell culture and centrifuged. 50 µl of the centrifuged culture medium was transferred to a 96 wells plate (5 replicates for each condition), added 50 µl of reaction mix and incubated for 15 minutes at room temperature, protected from light. 50 µl stop solution was used to stop the reaction. Plates were shaken briefly before reading the absorbance at 490 nm in an iMark microplate absorbance reader (BioRad).

6.7.1 Apoptosis assay - Principle

One of the major effects of radiation on osteocyte-like cell lines is the induction of apoptosis. (45) As such, the rate of apoptosis of irradiated MLO-Y4 cells was compared in both static and fluid flow conditions to assess the protective effects of mechanical load in the form of fluid flow. Apoptosis takes place through the activation of the caspase cascade. (49) Levels of apoptosis can therefore be determined through measuring the caspase activity inside the cells. Using the Caspase-Glo 3/7 assay (Promega, USA), the cells were lysed and a caspase substrate was added. Caspases 3 and 7, both apoptosis executioners, convert the substrate into aminoluciferin, which can be converted into a luminescent signal in the presence of luciferase.

6.7.2 Apoptosis assay - Protocol

Caspase-Glo 3/7 reagent was added in equal volume to the cell culture medium and incubated for one hour at room temperature, either 2 or 24 hours after irradiation immediately followed by either static or fluid flow treatment. Luminescence was measured using a Victor2 luminometer (PerkinElmer)

6.8 Quantification of Gene Expression

Most cells initial response to a change in their (micro)environment is a change in gene expression. A cascade of signalling molecules will lead to the production of mRNA, the first step in the synthesis of a protein. It is therefore a common practice to investigate a cells response to an environmental factor by measuring a change in mRNA expression levels within the cells. During a quantitative reverse-transcription polymerase chain reaction (qRT-

PCR), the amount of mRNA of a gene of interest is compared to the amount of mRNA of a constantly and stable expressed “housekeeping gene” to measure the changes in relative gene expression, making it a semiquantitative measure.

6.8.1 RNA Isolation – Principle

After lysation of the cells the total RNA is isolated by applying the cell-lysate to a spin column containing a porous membrane. The spin column is repeatedly centrifuged after addition of various solvents. In the last centrifugation step the total RNA is eluted from the membrane and dissolved in RNase-free water. The yield of the isolation, and any DNA or protein contamination, was determined using a DeNovix DS-11+ Spectrophotometer. Absorbance was measured at 230, 260 and 280 nm. The sample was considered “free of contamination” when the of the absorbance at 260 nm was 2.00 times higher than the absorbance at 280 nm and 1.80 times higher than the absorbance at 230 nm.

6.8.2 cDNA Synthesis – Principle

The isolated RNA is used to synthesise the complementary DNA (cDNA) necessary for the qRT-PCR. Total cell number is corrected for by using equal total amounts of RNA for the cDNA synthesis. The cDNA synthesis is catalysed by a reverse transcriptase, which uses mRNA as a template for the production of cDNA.

6.8.3 Quantitative reverse-transcription polymerase chain reaction (qRT-PCR) – Principle

During the qPCR, DNA polymerase is used to amplify the amount of cDNA. The reaction mixture is cyclically heated and cooled down to allow for multiple cycles of DNA strand dissociation, primer association and DNA polymerization. The amount of double stranded DNA can be determined by the addition of a SYBR green dye. This dye binds double stranded DNA to give a detectable luminescent signal. The dissociation and polymerization are repeated cyclically until a threshold value is reached. Each additional cycle required to reach the threshold value corresponds to half as much starting cDNA. (54, 55)

6.8.4 RNA Isolation – Protocol

The cells were lysed and the total RNA was isolated using the RNeasy mini kit (Qiagen, Germany). The cells were disrupted using 350 µl RLT buffer containing 1% β-mercaptoethanol the samples were homogenized by passing 5-10 times though a 20-gauge

needle. Lysates were mixed with an equal volume of 70% ethanol and 700 µl of the sample was applied to the RNeasy mini column. The column centrifuged for 15 second. 700 µl RW1 buffer was added to the column followed by 15 seconds of centrifugation. 500 µl RPE buffer was twice added followed by centrifugation. The first time for 15 seconds and the second time for 2 minutes. The column was centrifuged a third time for 60 seconds without the addition of RPE buffer. The total RNA was eluted from the column by adding 20 µl of RNase-free water and centrifuging for 60 seconds. All centrifugations were at 13400 rpm.

6.8.5 cDNA Synthesis – Protocol

cDNA was synthesised from the total RNA using the maxima first strand cDNA synthesis kit (Thermo Scientific). The isolated total RNA was diluted to 100 ng in 14 µl. Four µl 5X reaction mix and 2 µl maxima reverse transcriptase enzyme were added to each sample and incubated for 10 minutes at room temperature. The samples were incubated for 15 minutes at 50 °C, after which the reaction was terminated by a 5 minute incubation at 85 °C. Both oligo$(dT)_{18}$ and random hexamer primers were used for the cDNA synthesis. All cDNA samples were diluted 1:3 with water before performing the RT-PCR.

6.8.6 Quantitative reverse-transcription polymerase chain reaction (qRT-PCR) - Protocol

To determine the mRNA levels, cDNA, primers (Table 1.) and PerfeCTa SYBR green FastMix (QuantaBio, USA) were added together to reach a total volume of 20 µl. Real-Time PCR was performed on StepOne Real-Time PCR system (Applied Biosystems, USA). The reaction mixture was activated by heating to 95 °C for 10 minutes. The qPCR took place over 40 cycles of 15 seconds at 95 °C, to dissociate the two DNA strands, and 60 seconds at 60 °C, to allow the primer to associate with the single stranded DNA. After the last cycle, a melt point curve was established by heating the mixture from 60 °C to 95 °C.

Table 1. Primer mixes used for quantitative RT-PCR.

Target Gene	Primer mix assay ID / primer sequence	manufacturer
GAPDH	Forward: AATGGGGTGAGGCCGGTGCT Reverse: CACCCTTCAAGTGGGCCCCG	Sigma
RANKL	qMmuCID0026078	Biorad
OPG	qMmuCID0027158	Biorad
Piezo1	Forward: ATCTGGGCCAGGCTATTTGG Reverse: ATCATGGCAATCAGGGCACA	Biorad
SOST	qMmuCED0045167	Biorad
Wnt1	qMmuCED0046180	Biorad
Wnt3a	Forward: TAGATGGGTGCGACCTGTTG Reverse: GAACCCTGCTCCCGTGTTAG	Biorad
Bax	qMmuCID0006274	Biorad
Bcl2	qMmuCED0039968	Biorad

6.9 Statistical Analysis

All statistical testing was done using SPSS 26.0 (SPSS Inc., USA). All values are presented as mean ± standard deviation (SD). Differences were evaluated using the Student's t-test and considered significant at $p < 0.05$.

7. Results

7.1 Radiation induces cell death

The MLO-Y4 osteocytes were irradiated with a dose of 5 Gy before the levels of cell death were investigated using ELISA targeting for oligonucleosomes, an indication of cell death. ELISA was performed 24 and 48 hours after the radiation of the cells (Figure 2). At both 24 hours and 48 hours after irradiation, the irradiated cells displayed significantly higher cell death ($p=0.008$ and $p<0.001$, respectively).

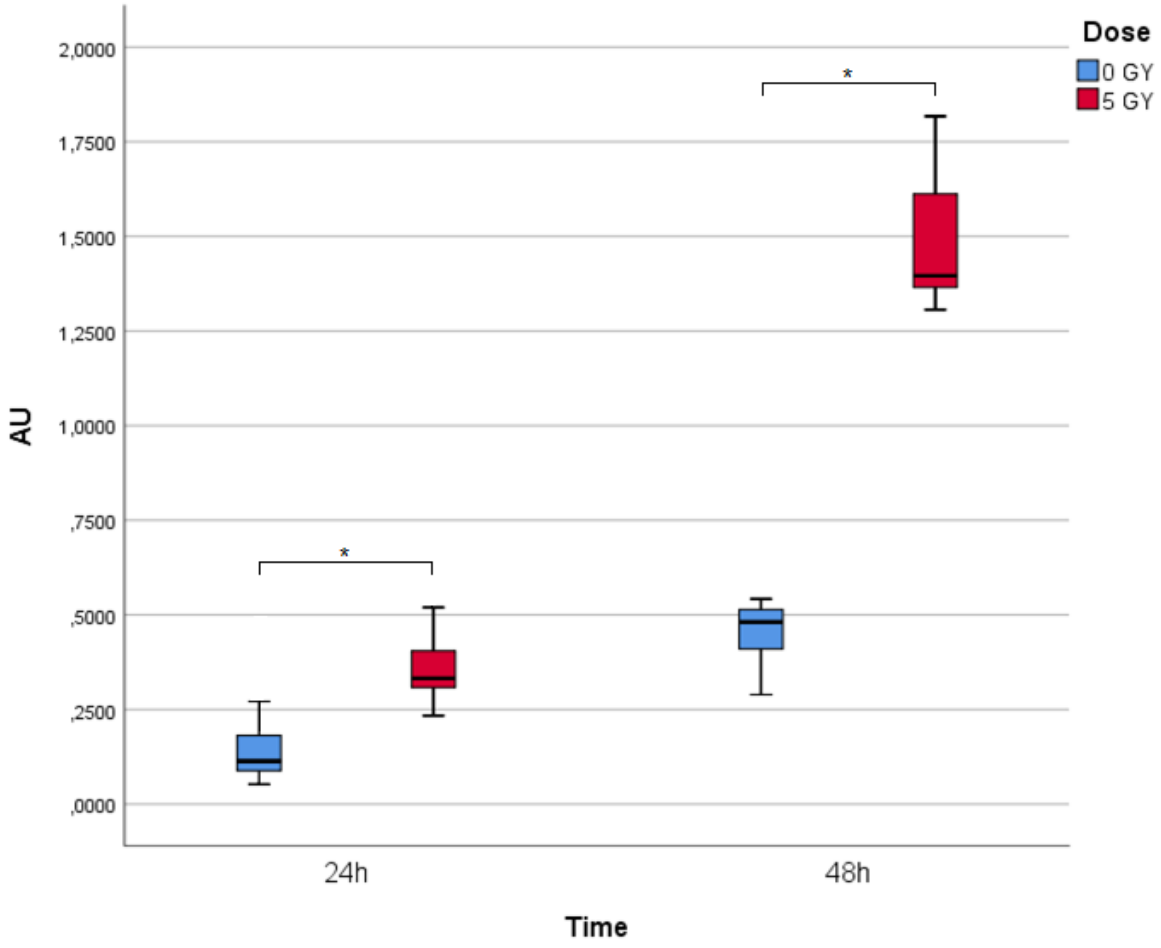

Figure 2: Radiation induced cell death as determined by quantification of oligonucleosomes. After 24 hours, non-irradiated cells (Absorbance 0.1415 ± 0.09) displayed significantly lower levels of cell death than the irradiated cells (Absorbance 0.3597 ± 0.11). After 48 hours, non-irradiated cells (Absorbance 0.4472 ± 0.10) again showed significantly lower levels of cell death than the irradiated cells (Absorbance 1.4992 ± 0.21). Results are displayed as mean ± SD (n=5). *-sign is used to signify significant differences ($p<0.05$). Abbreviations: AU is arbitrary unit for absorbance, h is hours.

MTT and LDH assays were performed to verify that 5Gy radiation causes cell death 24 hours after radiation (Figure 3). MTT assays were performed 2, 24, 48, 72, and 120 hours after radiation to determine how long after irradiation the cell viability decreased (Figure 3, Left). Cell viability significantly decreased after 48 and 72 hours ($p=0.018$ and $p<0.001$ respectively). 120 hours after irradiation, mitochondrial activity of the irradiated samples was significantly higher than that of the non-irradiated samples ($p=0.009$).

LDH assays were also performed at 2, 24, 48, 72, and 120 hours after irradiation of the samples to determine extracellular LDH activity. (Figure 3, Right) LDH activity of irradiated cells compared to non-irradiated cells followed a similar pattern as measured by the MTT assays, although the difference between radiated and non-radiated cells was at none of the measured time points significant. The determined p-values were 0.077 and 0.058 and 0.055 at 48h, 72h, and 120h respectively. During a second experimental set-up, LDH assays were performed 24 and 48 hours after the radiation of the cells. The extracellular LDH activity was significantly higher both 24 hours ($p=0.001$) and 48 hours ($p=0.013$) after radiation.

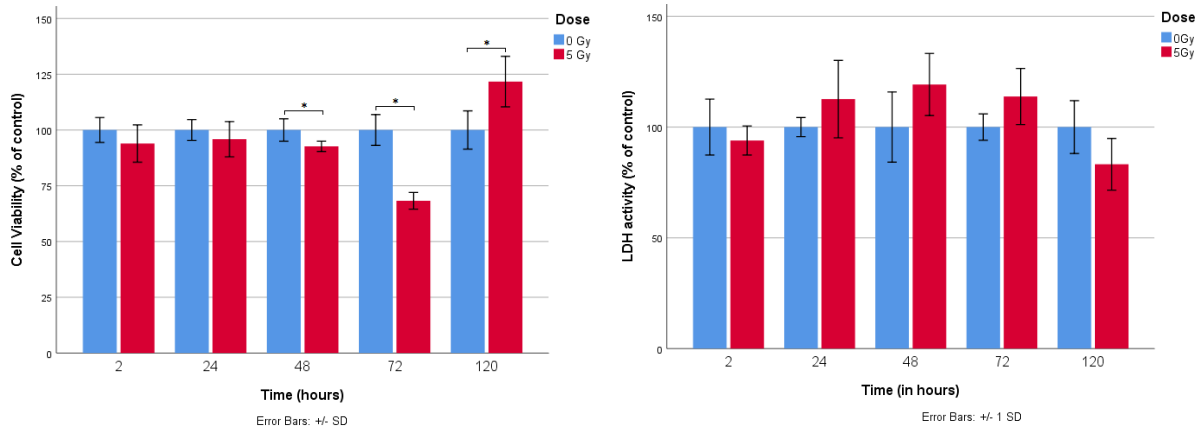

Figure 3: Cell viability and extracellular LDH activity of MLO-Y4 cells after radiation as a percentage of control.

Left: cell viability as measured by MTT assay. After 48 and 72 hours, irradiated samples had significantly lower cell viability. After 120 hours cell viability of the irradiated cells was higher than that of the control. Results are displayed as mean percentage of control ± SD (n=5). *-sign is used to signify significant differences ($p<0.05$).

Right: extracellular LDH activity as measured by LDH assay. Increased extracellular LDH activity indicates increased plasma membrane damage. LDH activity increases 24, 48, and 72 hours after radiation, but increases 2 and 120 hours after radiation. None of the differences are

significant. Results are displayed as mean percentage of control ± SD (n=5). Differences with a $p<0.05$ are considered significant.

7.2 The effect of radiation on gene expression in MLO-Y4 osteocytes

To further elucidate the response of osteocytes on radiation, we investigated changes in gene expression in response to radiation. RANKL and OPG, two regulators of osteoclastogenesis, were followed 2, 24, and 48 hours after radiation. OPG expression did not change significantly in response to radiation whereas RANKL expression increased significantly after 24 and 48 hours in one experiment ($p=0.04$ and $p=0.002$). When the experiment was replicated, RANKL expression seemed to increase, but not significantly ($p=0.3$ and $p=0.4$). Changes in RANKL and OPG expression are represented as the ratio of RANKL/OPG, since osteoclastogenesis is regulated by the shift in balance between RANKL and OPG expression (Figure 4).

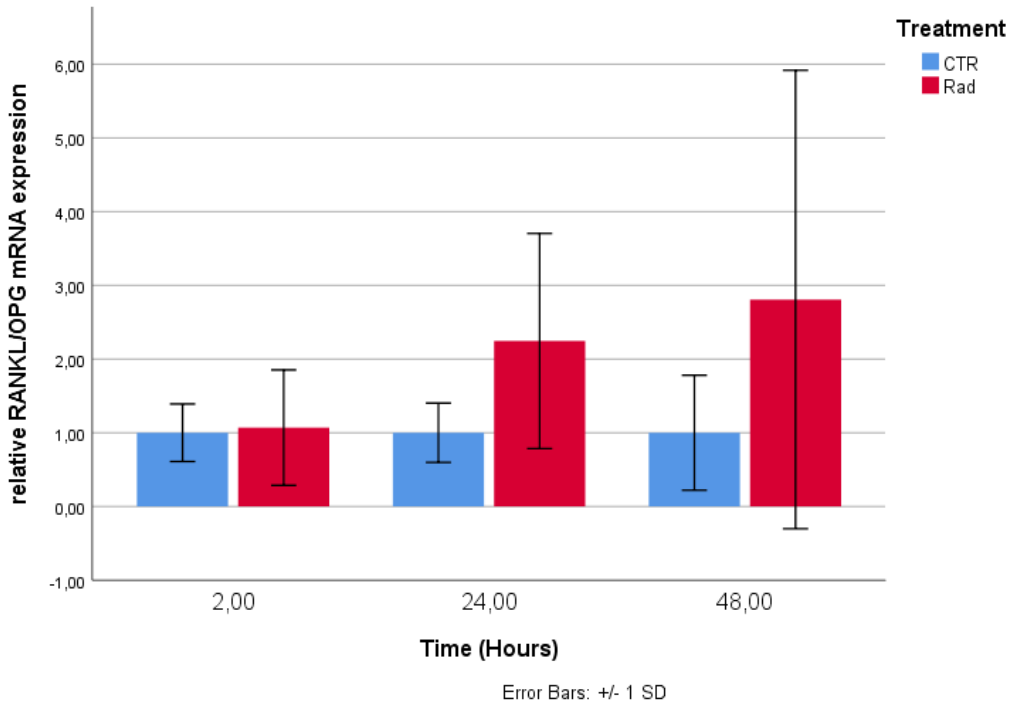

Figure 4: Relative expression of RANKL/OPG mRNA expression compared to control.
A visible but insignificant shift in RANKL/OPG mRNA expression was shown 24 and 48 hours after 5 Gy radiation treatment. Results are represented as mean compared to control ± SD (n=6). Abbreviations: CTR is non-radiated control, Rad is radiated cells

Additionally, changes in expression of Piezo1, SOST, Wnt1, Wnt3a, Bcl2, and Bax were all investigated 2h, 24h and 48 hours after radiation. The experiment was repeated three times with inconsistent results (Figure 5-10).

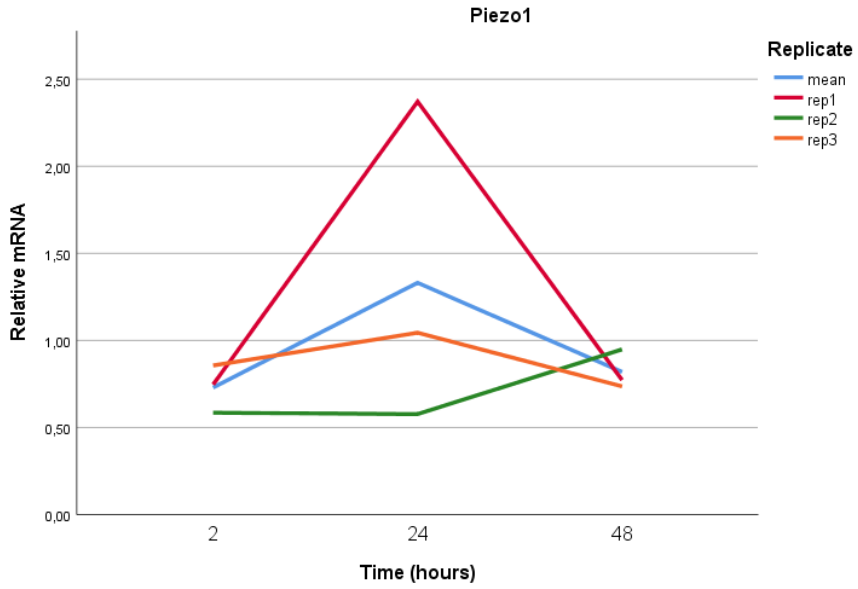

Figure 5: expression of Piezo1 mRNA after radiation relative to control.

Replicate 1 (red) displayed a significant drop after 2 hours, followed by a significant increase after 24 hours before going back to similar levels of expression compared to control after 48 hours. Replicate 2 (green) displayed decreased expression of Piezo1 compared to control 2 and 24 hours after radiation. Replicate 3 (orange) did not differ significantly from the non-radiated control. The mean of the three replicates in displayed in blue.

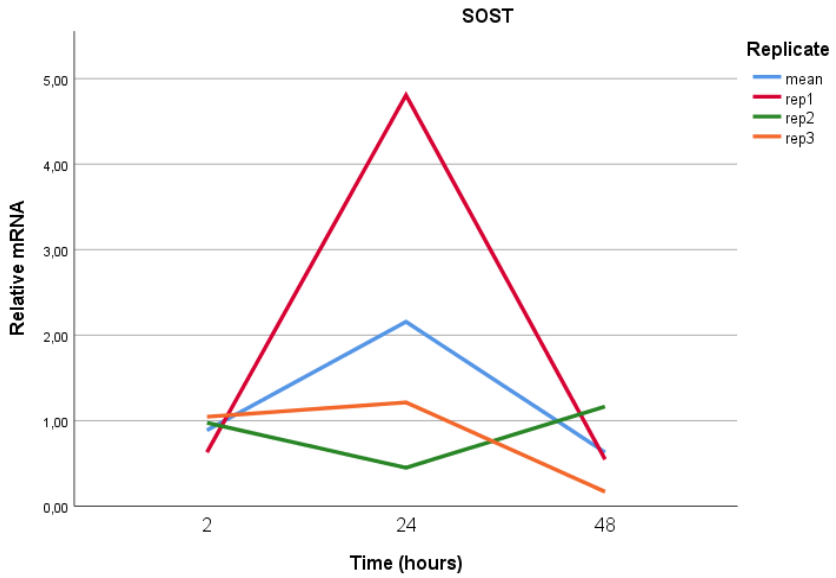

Figure 6: expression of SOST mRNA after radiation relative to non-radiated control.

Replicate 1 (red) expressed SOST in response to radiation following a similar pattern as Piezo1, decreasing 2 hours after radiation and increasing 24 hours after radiation. Replicates 2 and 3 (green and orange) showed no significant change in SOST expression in response to radiation. The mean of all replicates is displayed in blue.

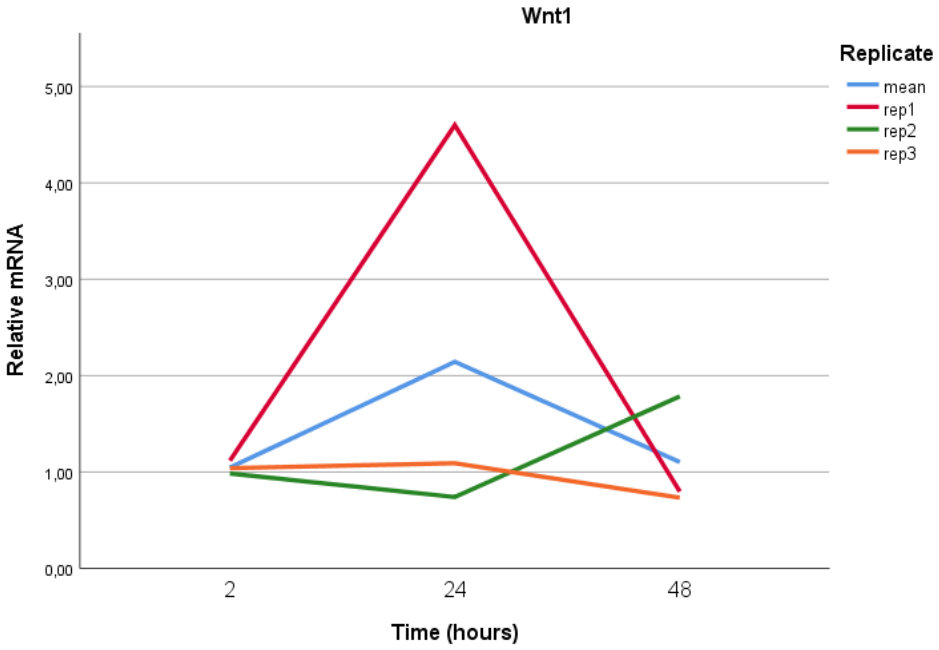

Figure 7: expression of Wnt1 mRNA after radiation relative to non-radiated control.

Replicate 1 (red) showed a significant increase in Wnt1 expression 24 hours after radiation. Replicates 2 and 3 (green and orange) showed no significant difference compared to the non-radiated control. Mean of the three replicates is displayed in blue.

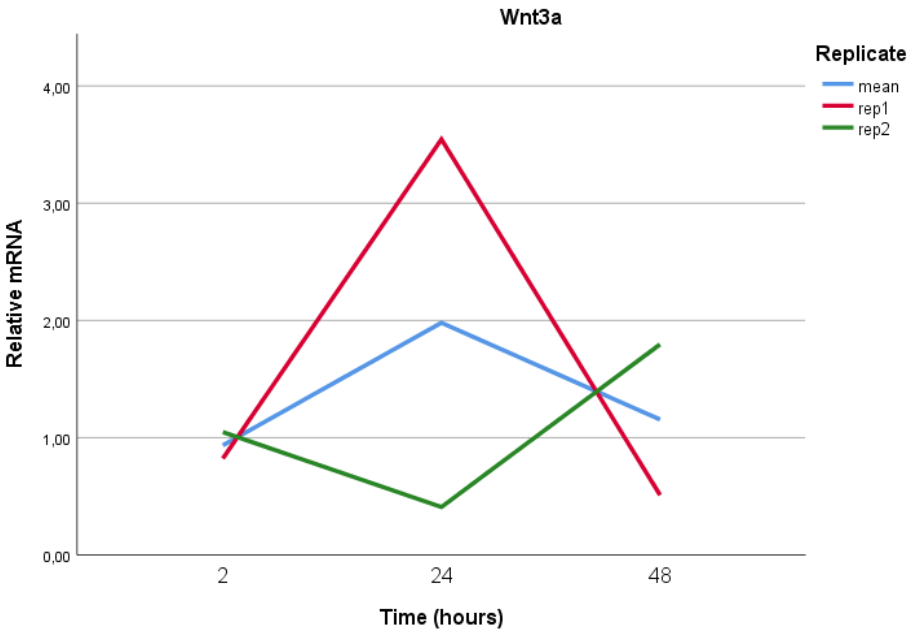

Figure 8: expression of Wnt3a mRNA after radiation relative to non-radiated control.

Replicate 1 (red) showed a significant increase in Wnt3a expression 24 hours after radiation. Replicate 2 (green) showed no significant difference compared to the non-radiated control. Mean of the two replicates is displayed in blue.

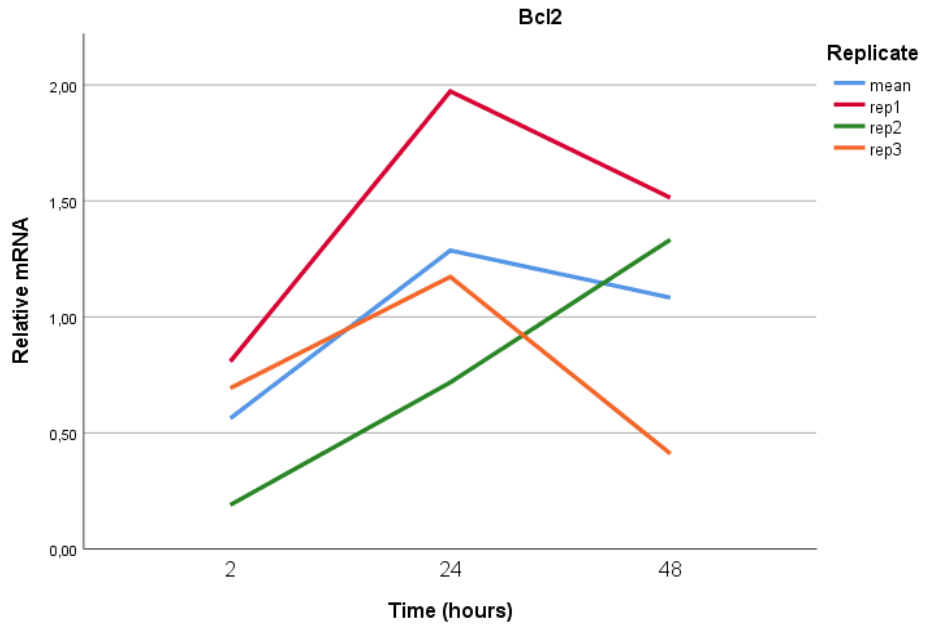

Figure 9: expression of Bcl2 mRNA after radiation relative to non-radiated control.

Expression of Bcl2 increased 24 and 48 hours after radiation for replicate 1 (red), but not for replicates 2 and 3 (green and orange). Mean of the three replicates is shown in blue.

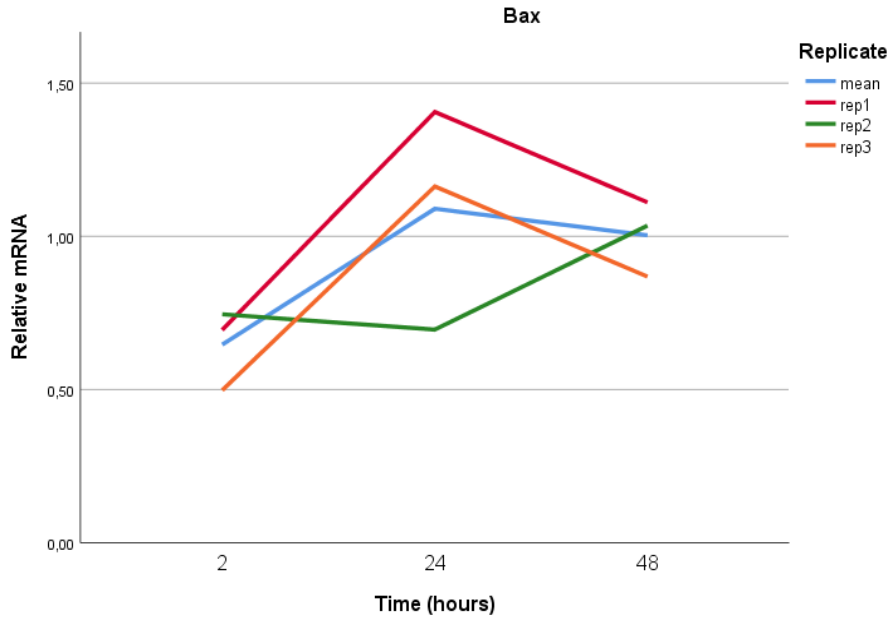

Figure 10: expression of Bax mRNA after radiation relative to non-radiated control.

Expression of Bax did not significantly change compared to control in any of the replicates. Replicates 1, 2, 3, and the mean of all replicates are displayed in red, green, orange and blue respectively.

7.3 Validation of the fluid flow experimental set up

The effectiveness of the experimental fluid flow set up to simulate mechanical loading of the osteocytes was assessed by investigating the increase of PGE2 protein expression in response to fluid flow. PGE2 expression is used as a marker for successful simulation of mechanical load since PGE2 expression is induced by mechanical loading of osteocytes. (21) ELISA for PGE2 was performed on the cell culture medium of cells exposed to fluid flow either 2 hours, 24 hours or 48 hours after fluid flow treatment. Fluid flow significantly increased PGE2 expression after all three measured time points ($p<0.001$), indicating that the experimental set up induced a response similar to that of mechanical load (Figure 11).

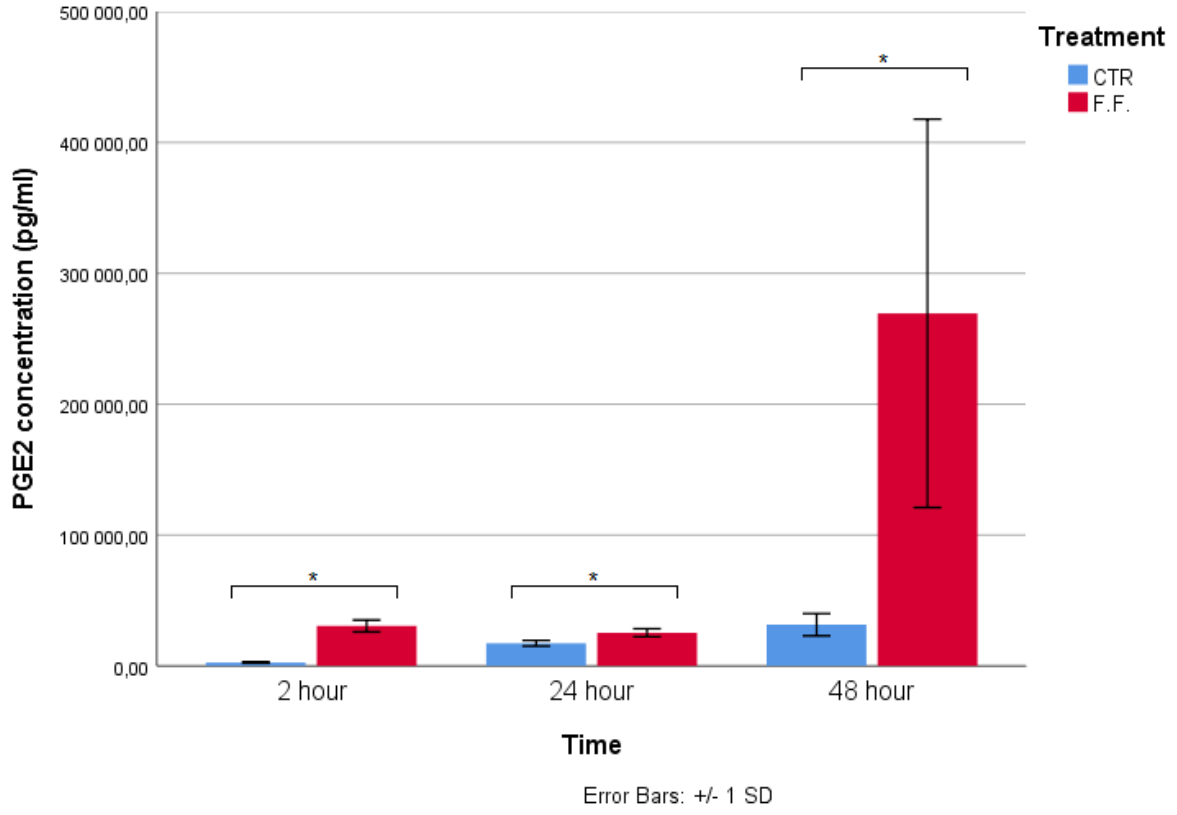

Figure 11: PGE2 expression in response to fluid flow.

Fluid flow significantly increased PGE2 expression (at all three time points $p<0.001$). Results are shown as mean concentration ± SD (n=6). *-sign is used to signify significant differences ($p<0.05$). Abbreviations: F.F. fluid flow treatment group. CTR control group.

7.4 Fluid flow alleviates radiation-induced apoptosis in MLO-Y4 osteocytes

To investigate the possible effects of fluid flow on radiation-induced apoptosis, MLO-Y4 cells were subjected to 5 Gy radiation and subsequently subjected to fluid flow shear stress and compared to a control group that did not undergo fluid flow shear stress. Caspase Glo-3/7

assay was performed 2 and 24 hours after treatment to assess apoptosis. Cells subjected to fluid flow shear stress exhibited significantly lower caspase activity (Figure 12).

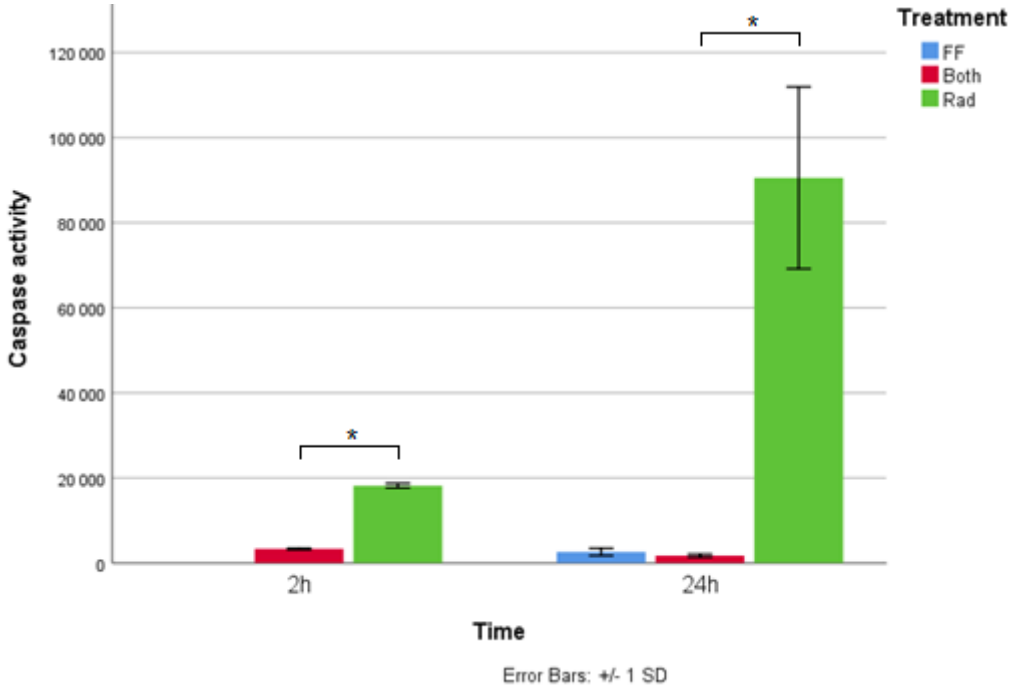

Figure 12: Caspase activity in response to radiation, fluid flow shear stress, or both as measured using Caspase 3/7 Glo-assay.

Cells subjected to radiation but not fluid flow shear stress exhibited significantly more caspase activity than the cells subjected to fluid flow shear stress or both radiation and fluid flow shear stress. Cells subjected to both fluid flow shear stress and radiation showed similar levels of caspase activity as cells not subjected to radiation. *-sign is used to signify significant differences ($p<0.05$). Results are displayed as mean ± SD (n=2, where both biological replicates used 4 to 7 technical replicates per sample). Experiment was performed twice, one representative result is displayed.

7.5 The combined effects of radiation and fluid flow on gene expression in MLO-Y4 osteocytes

The expression of RANKL and OPG mRNA in response to fluid flow after radiation was investigated to study the effects of fluid flow shear stress on osteocyte-mediated osteoclast regulation. RANKL mRNA expression slightly decreased 2 hours after radiation and fluid flow compared to the radiated control. After 48 hours RANKL expression had slightly increased compared to control. Expression of OPG greatly increased in response to fluid flow, leading to a decrease in RANKL:OPG ratio (Figure 13).

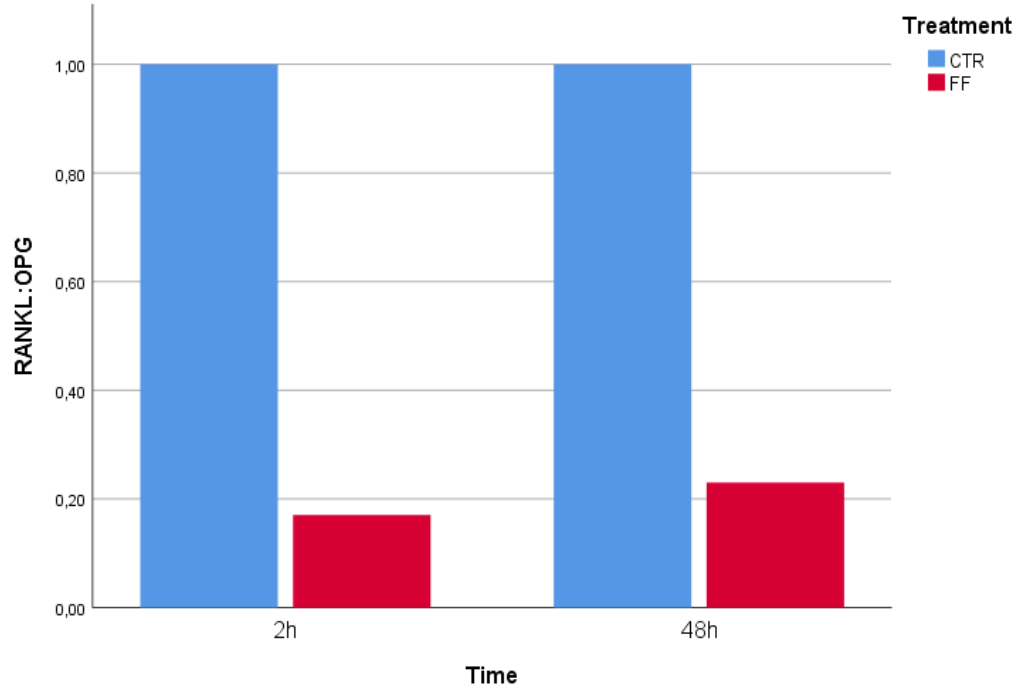

Figure 13: Changes in RANKL:OPG ratio in response to fluid flow after radiation relative to control.

RANKL:OPG ratio had decreased roughly 5 fold compared to the radiated control 2 hours after fluid flow. This decrease persisted for at least 48 hours. Statistical analysis was inapplicable due to the lack of replicates (n=1).

Additionally, expression of SOST, Bcl2 and Bax expression in response to fluid flow after radiation were determined 2 hours, 24 hours and 48 hours after fluid flow treatment and compared to radiated control (Table 2).

Table 2: Expression of SOST, Bcl2 and Bax mRNA in response to fluid flow.

mRNA expression is represented as compared to radiated control. Expression of SOST greatly increased 24 hours after fluid flow treatment before decreasing again. Bcl2 expression increased 50-fold 24 and 48 hours after fluid flow treatment. Bax expression decreased sharply 24 hours after fluid flow treatment before slowly increasing again, leading to an increase in Bcl2:Bax ratio, which inhibits apoptosis.

Time	SOST	Bcl2	Bax	Bcl2:Bax
2 hours	6.339	1.735	1.053	1.647
24 hours	407.114	50.608	0.004	14395.075
48 hours	89.526	49.231	0.147	335.140

8. Discussion of methodology and results

8.1 Discussion of methodology

Osteocytes were the primary focus of this study, as these are the main cell type involved in the perception of mechanical stress in bone tissue. (9, 20) Osteocytes differ from osteoblast due to the osteocytes dendritic morphology and lower expression of ALP, combined with a higher expression of connexin43 and higher secretion of osteocalcin. (56) The two most widely used osteocyte-like cell lines are MLO-Y4 and MLO-A5, because these cell lines can still undergo proliferation. (57) MLO-Y4 cells have previously been used to study cell death and apoptosis whereas MLO-A5 cells are the cell line of choice for the purpose of studying mineralization. (45, 58) This, together with the high sensitivity of MLO-Y4 cells to fluid flow shear stress, made MLO-Y4 the cell line of choice for this study. (57)

Previous studies have shown that growth medium containing both fetal bovine serum (FBS) and calf serum (CS) lead to an optimal balance between cell proliferation and cell differentiation of osteocyte-like cells, especially when grown on a collagen type 1 coated surface. (56) Additionally, osteocyte cultured medium contains factors that act on the later phases of osteoblastic cell line differentiation. (59) A fluid flow regime with a force of 10 dynes/cm^2 over 2 hours was used, as this regime had previously been shown to induce a change in gene expression in previous studies, where it increased the production of nitric oxide and PGE_2 through increased expression of Ptgs2, iNOS and Nos2. (60, 61) Unlike the cited studies, the used fluid flow regime did not employ oscillating fluid flow. Despite not interfering with PGE_2 expression, use of oscillating fluid flow would be more similar to physiological conditions and possible hidden differences cannot be excluded. Moreover, the employed fluid flow set up only allowed for 6 slides with cells to be subjected to fluid flow. This severely limited the number of replicates for each experiment.

Typical radiotherapy regimes for colorectal cancer patients involve a radiation dose of 2 Gy per day, five days per week. However, previous studies on MLO-Y4 cells have shown a single dose of 2 Gy to be insufficient to induce a response within 72 hours. (45) A dose of 5 Gy was decided upon, which had been shown previously to change cell morphology and decrease cell viability in MLO-Y4 cells. (45, 46) Multiple assays were used to investigate cell damage as a result of radiation, since differing cytotoxicity assays can give differing results. (51) This combination of MTT assays, LDH assays and ELISA gave reliable evidence that 5

Gy radiation was a high enough dose to induce cell damage within 48 hours. The Caspase 3/7 Glo assay was used to assess apoptotic activity after fluid flow treatment as it gave a more specific image of the mechanism through which fluid flow shear stress protects osteocytes. The qPCR results following radiation show a large variation between replicates, leading to a high standard deviation in RANKL:OPG ratios. Additional replicates may have given a more conclusive outcome. The qPCR study into the combined effect of radiation and fluid flow only contained one replicate, making statistical analysis impossible and severely limiting the reliability of the conclusions drawn from its findings.

8.2 Discussion of results

The cell death ELISA targeting fragmented DNA and histones showed a significant increase in cell death after 24 hours (Figure 2), whereas the MTT assay did not show any significant differences before 48 hours (Figure 3). This could possibly be explained by the fact that DNA double strand breaks are a direct result of radiation, with DNA damage being the primary mechanism through which radiation induces cell death. (62) This might explain why fragmented DNA is significantly increased before mitochondrial activity decreases. Nevertheless, the finding that 5 Gy radiation causes cell death within 48 hours after treatment seems to be in agreement with previous studies done on MLO-Y4 osteocytes. (45, 46)
After 120 hours, cell death seems to be lower in the radiated cells than the non-radiated controls (Figure 3). The non-radiated cells could have possibly grown overconfluent, leading to changed morphology and decreased cell viability compared to the radiated cells.
Both LDH assay and MTT assay displayed a similar pattern of radiation induced damage, but only the MTT assay gave significant differences between radiated cells and the non-radiated controls after 48 hours. The MTT assay has been shown to be more sensitive than the LDH assay, generally requiring lower doses and shorter incubation times of cytotoxic agents before measuring significant amounts of cytotoxicity. (51, 63)
Gene expression of RANKL increased in response to radiation, whereas none of the other investigated genes changed significantly. The increase in RANKL gene expression is in accordance with a recent study by He et al. on the effect of radiation on osteocytes. (45) In this study, the gene expression of OPG had also decreased as a result of radiation, however this was 72 hours after radiation treatment. As seen in the study by He et al., the ratio in RANKL:OPG gene expression increased (Figure 4), although the large standard deviation caused the increase to be insignificant. (45)
Osteocytes subjected to Fluid flow shear stress following the radiation showed significantly

decreased apoptotic activity compared to radiated osteocytes, suggesting that mechanical loading attenuates the effects of radiation on osteocytes. This may in part be due to the activation of PGE_2 in response to fluid flow shear stress (Figure 11), which activates β-catenin signalling and increases cell survival. In addition to increased PGE_2 excretion, the ratio of Bcl2:Bax gene expression increased (Table 2), further inhibiting apoptosis. Fluid flow after radiation treatment decreased the ratio of RANKL:OPG gene expression 5 fold (Figure 13), suggesting that fluid flow reduces radiation induced osteocyte-mediated activation of osteoclast, further protecting bone strength. However, fluid flow also increased SOST expression, in turn inhibiting osteoblast activity and negatively impacting bone strength. This result does contradict previous findings that mechanical loading of osteocytes decreases SOST expression, while increasing Wnt-signalling. (20, 27) It would therefore be interesting to investigate the effect of fluid flow following radiation on the expression of canonical Wnt-ligands and to determine if there is a net increase or decrease of Wnt-signalling due to fluid flow.

9. Conclusion

Recent research has shown the protective effects of mechanical loading on bone. This *in vitro* study investigates the possible protective effects of mechanical loading against radiation induced damage of osteocytes. In summary, a radiation dose of 5 Gy was shown to induce cell death within 24 to 48 hours after treatment. Additionally, radiation increased the expression of RANKL, a factor that increases osteoclast activity. When radiation is followed by fluid flow shear stress to mimic mechanical loading, the cells display significantly lower levels of apoptosis. Additionally, the RANKL:OPG ratio decreased, leading to less osteoclast activation, whereas the ratio of Bcl2:Bax increases. Together with the fluid flow induced increase in PGE_2 excretion, this increase in Bcl2:Bax could be a possible explanation for the decrease in apoptosis. These results support the hypothesis that mechanical loading by exercise during and after radiotherapy could help in the protection against cancer treatment induced bone loss, which could have great clinical implications in the prevention of osteoporosis if proven correct. This study is part of a larger project and it will be interesting to see if these *in vitro* results are in agreement with the animal study and patient study, in which the effects of exercise and radiotherapy on bone health are investigated. In the gene expression experiments, one of the three replicates seemed to diverge from the other replicates and additional future experiments are needed to draw reliable conclusions from these results (Figures 5-10). Future *in vitro* studies are needed to investigate whether fluid

flow after radiation leads to a net increase or decrease in osteoblast-activating Wnt-signalling. Additionally, studies on the effects of Piezo1 and its downstream targets could further elucidate the mechanism through which fluid flow protects osteocytes from radiation induced apoptosis.

10. References

1. Tsao Y, Creedy DK. Auricular acupressure: reducing side effects of chemotherapy in women with ovarian cancer. Support Care Cancer. 2019;27(11):4155-63.
2. Liu Y, Wang H, Deng J, Sun C, He Y, Zhou C. Toxicity of tumor immune checkpoint inhibitors-more attention should be paid. Transl Lung Cancer Res. 2019;8(6):1125-33.
3. Islam KM, Anggondowati T, Deviany PE, Ryan JE, Fetrick A, Bagenda D, et al. Patient preferences of chemotherapy treatment options and tolerance of chemotherapy side effects in advanced stage lung cancer. BMC Cancer. 2019;19(1):835-.
4. Stewart SA, Yao Z, Murali B, Ren Q, Luo X, Faget DV, et al. Therapy-induced senescence drives bone loss. Cancer Res. 2020.
5. D'Oronzo S, Stucci S, Tucci M, Silvestris F. Cancer treatment-induced bone loss (CTIBL): pathogenesis and clinical implications. Cancer Treat Rev. 2015;41(9):798-808.
6. Chandra A, Lin T, Tribble MB, Zhu J, Altman AR, Tseng WJ, et al. PTH1-34 alleviates radiotherapy-induced local bone loss by improving osteoblast and osteocyte survival. Bone. 2014;67:33-40.
7. Datta HK, Ng WF, Walker JA, Tuck SP, Varanasi SS. The cell biology of bone metabolism. J Clin Pathol. 2008;61(5):577-87.
8. Clarke B. Normal bone anatomy and physiology. Clinical journal of the American Society of Nephrology : CJASN. 2008;3 Suppl 3(Suppl 3):S131-S9.
9. Florencio-Silva R, Sasso GR, Sasso-Cerri E, Simoes MJ, Cerri PS. Biology of Bone Tissue: Structure, Function, and Factors That Influence Bone Cells. BioMed research international. 2015;2015:421746.
10. Ono T, Nakashima T. Recent advances in osteoclast biology. Histochem Cell Biol. 2018;149(4):325-41.
11. Cappariello A, Maurizi A, Veeriah V, Teti A. The Great Beauty of the osteoclast. Arch Biochem Biophys. 2014;558:70-8.
12. Boyce BF. Advances in the regulation of osteoclasts and osteoclast functions. J Dent Res. 2013;92(10):860-7.
13. Chen X, Wang Z, Duan N, Zhu G, Schwarz EM, Xie C. Osteoblast-osteoclast interactions. Connect Tissue Res. 2018;59(2):99-107.
14. Mulari M, Vaaraniemi J, Vaananen HK. Intracellular membrane trafficking in bone resorbing osteoclasts. Microsc Res Tech. 2003;61(6):496-503.

15. Fakhry M, Hamade E, Badran B, Buchet R, Magne D. Molecular mechanisms of mesenchymal stem cell differentiation towards osteoblasts. World J Stem Cells. 2013;5(4):136-48.
16. Capulli M, Paone R, Rucci N. Osteoblast and osteocyte: games without frontiers. Arch Biochem Biophys. 2014;561:3-12.
17. Pi M, Quarles LD. Novel bone endocrine networks integrating mineral and energy metabolism. Curr Osteoporos Rep. 2013;11(4):391-9.
18. Komori T, Yagi H, Nomura S, Yamaguchi A, Sasaki K, Deguchi K, et al. Targeted Disruption of Cbfa1 Results in a Complete Lack of Bone Formation owing to Maturational Arrest of Osteoblasts. Cell. 1997;89(5):755-64.
19. Bonewald LF. The amazing osteocyte. J Bone Miner Res. 2011;26(2):229-38.
20. Goldring SR. The osteocyte: key player in regulating bone turnover. RMD Open. 2015;1(Suppl 1):e000049.
21. Fritton SP, Weinbaum S. Fluid and Solute Transport in Bone: Flow-Induced Mechanotransduction. Annu Rev Fluid Mech. 2009;41:347-74.
22. Piekarski K, Munro M. Transport mechanism operating between blood supply and osteocytes in long bones. Nature. 1977;269(5623):80-2.
23. Cowin SC, Weinbaum S, Zeng Y. A case for bone canaliculi as the anatomical site of strain generated potentials. J Biomech. 1995;28(11):1281-97.
24. Weinbaum S, Cowin SC, Zeng Y. A model for the excitation of osteocytes by mechanical loading-induced bone fluid shear stresses. J Biomech. 1994;27(3):339-60.
25. Wang Y, McNamara LM, Schaffler MB, Weinbaum S. A model for the role of integrins in flow induced mechanotransduction in osteocytes. Proc Natl Acad Sci U S A. 2007;104(40):15941-6.
26. Santos A, Bakker AD, Zandieh-Doulabi B, de Blieck-Hogervorst JMA, Klein-Nulend J. Early activation of the β-catenin pathway in osteocytes is mediated by nitric oxide, phosphatidyl inositol-3 kinase/Akt, and focal adhesion kinase. Biochem Biophys Res Commun. 2010;391(1):364-9.
27. Li X, Han L, Nookaew I, Mannen E, Silva MJ, Almeida M, et al. Stimulation of Piezo1 by mechanical signals promotes bone anabolism. Elife. 2019;8.
28. Joeng KS, Lee YC, Lim J, Chen Y, Jiang MM, Munivez E, et al. Osteocyte-specific WNT1 regulates osteoblast function during bone homeostasis. J Clin Invest. 2017;127(7):2678-88.

29. Mavcic B, Antolic V. Optimal mechanical environment of the healing bone fracture/osteotomy. Int Orthop. 2012;36(4):689-95.
30. Ehrlich PJ, Lanyon LE. Mechanical strain and bone cell function: a review. Osteoporos Int. 2002;13(9):688-700.
31. Yan Y, Wang L, Ge L, Pathak JL. Osteocyte-Mediated Translation of Mechanical Stimuli to Cellular Signaling and Its Role in Bone and Non-bone-Related Clinical Complications. Curr Osteoporos Rep. 2020.
32. Jiang JX, Cheng B. Mechanical stimulation of gap junctions in bone osteocytes is mediated by prostaglandin E2. Cell Commun Adhes. 2001;8(4-6):283-8.
33. Downey PA, Siegel MI. Bone Biology and the Clinical Implications for Osteoporosis. Phys Ther. 2006;86(1):77-91.
34. Matic I, Matthews BG, Wang X, Dyment NA, Worthley DL, Rowe DW, et al. Quiescent Bone Lining Cells Are a Major Source of Osteoblasts During Adulthood. Stem Cells. 2016;34(12):2930-42.
35. Matsuo K, Irie N. Osteoclast-osteoblast communication. Arch Biochem Biophys. 2008;473(2):201-9.
36. Negishi-Koga T, Shinohara M, Komatsu N, Bito H, Kodama T, Friedel RH, et al. Suppression of bone formation by osteoclastic expression of semaphorin 4D. Nat Med. 2011;17(11):1473-80.
37. Negishi-Koga T, Takayanagi H. Bone cell communication factors and Semaphorins. Bonekey Rep. 2012;1:183.
38. Hayashi M, Nakashima T, Taniguchi M, Kodama T, Kumanogoh A, Takayanagi H. Osteoprotection by semaphorin 3A. Nature. 2012;485(7396):69-74.
39. Zhao C, Irie N, Takada Y, Shimoda K, Miyamoto T, Nishiwaki T, et al. Bidirectional ephrinB2-EphB4 signaling controls bone homeostasis. Cell Metab. 2006;4(2):111-21.
40. Riggs BL. The mechanisms of estrogen regulation of bone resorption. The Journal of clinical investigation. 2000;106(10):1203-4.
41. Mohamad NV, Soelaiman IN, Chin KY. A concise review of testosterone and bone health. Clin Interv Aging. 2016;11:1317-24.
42. Vandenput L, Boonen S, Van Herck E, Swinnen JV, Bouillon R, Vanderschueren D. Evidence from the aged orchidectomized male rat model that 17beta-estradiol is a more effective bone-sparing and anabolic agent than 5alpha-dihydrotestosterone. J Bone Miner Res. 2002;17(11):2080-6.

43. Robertson JF, Blamey RW. The use of gonadotrophin-releasing hormone (GnRH) agonists in early and advanced breast cancer in pre- and perimenopausal women. Eur J Cancer. 2003;39(7):861-9.
44. Chengalvala MV, Pelletier JC, Kopf GS. GnRH agonists and antagonists in cancer therapy. Curr Med Chem Anticancer Agents. 2003;3(6):399-410.
45. He F, Bai J, Wang J, Zhai J, Tong L, Zhu G. Irradiation-induced osteocyte damage promotes HMGB1-mediated osteoclastogenesis in vitro. J Cell Physiol. 2019;234(10):17314-25.
46. Wright LE, Buijs JT, Kim HS, Coats LE, Scheidler AM, John SK, et al. Single-Limb Irradiation Induces Local and Systemic Bone Loss in a Murine Model. J Bone Miner Res. 2015;30(7):1268-79.
47. Farris MK, Helis CA, Hughes RT, LeCompte MC, Borg AM, Nieto K, et al. Bench to Bedside: Animal Models of Radiation Induced Musculoskeletal Toxicity. Cancers (Basel). 2020;12(2).
48. Chandra A, Lin T, Young T, Tong W, Ma X, Tseng WJ, et al. Suppression of Sclerostin Alleviates Radiation-Induced Bone Loss by Protecting Bone-Forming Cells and Their Progenitors Through Distinct Mechanisms. J Bone Miner Res. 2017;32(2):360-72.
49. Fan TJ, Han LH, Cong RS, Liang J. Caspase family proteases and apoptosis. Acta Biochim Biophys Sin (Shanghai). 2005;37(11):719-27.
50. Adams JM, Cory S. The Bcl-2 apoptotic switch in cancer development and therapy. Oncogene. 2007;26(9):1324-37.
51. Fotakis G, Timbrell JA. In vitro cytotoxicity assays: comparison of LDH, neutral red, MTT and protein assay in hepatoma cell lines following exposure to cadmium chloride. Toxicol Lett. 2006;160(2):171-7.
52. Kumar P, Nagarajan A, Uchil PD. Analysis of Cell Viability by the MTT Assay. Cold Spring Harb Protoc. 2018;2018(6).
53. Kumar P, Nagarajan A, Uchil PD. Analysis of Cell Viability by the Lactate Dehydrogenase Assay. Cold Spring Harb Protoc. 2018;2018(6).
54. Wagner EM. Monitoring gene expression: quantitative real-time rt-PCR. Methods Mol Biol. 2013;1027:19-45.
55. Freeman WM, Walker SJ, Vrana KE. Quantitative RT-PCR: pitfalls and potential. Biotechniques. 1999;26(1):112-22, 24-5.
56. Kato Y, Windle JJ, Koop BA, Mundy GR, Bonewald LF. Establishment of an osteocyte-like cell line, MLO-Y4. J Bone Miner Res. 1997;12(12):2014-23.

57. Kalajzic I, Matthews BG, Torreggiani E, Harris MA, Divieti Pajevic P, Harris SE. In vitro and in vivo approaches to study osteocyte biology. Bone. 2013;54(2):296-306.
58. Barragan-Adjemian C, Nicolella D, Dusevich V, Dallas MR, Eick JD, Bonewald LF. Mechanism by which MLO-A5 late osteoblasts/early osteocytes mineralize in culture: similarities with mineralization of lamellar bone. Calcif Tissue Int. 2006;79(5):340-53.
59. Heino TJ, Hentunen TA, Vaananen HK. Conditioned medium from osteocytes stimulates the proliferation of bone marrow mesenchymal stem cells and their differentiation into osteoblasts. Exp Cell Res. 2004;294(2):458-68.
60. Govey PM, Kawasawa YI, Donahue HJ. Mapping the osteocytic cell response to fluid flow using RNA-Seq. J Biomech. 2015;48(16):4327-32.
61. Xu H, Guan Y, Wu J, Zhang J, Duan J, An L, et al. Polycystin 2 is involved in the nitric oxide production in responding to oscillating fluid shear in MLO-Y4 cells. J Biomech. 2014;47(2):387-91.
62. Baskar R, Dai J, Wenlong N, Yeo R, Yeoh K-W. Biological response of cancer cells to radiation treatment. Front Mol Biosci. 2014;1:24-.
63. Weyermann J, Lochmann D, Zimmer A. A practical note on the use of cytotoxicity assays. Int J Pharm. 2005;288(2):369-76.

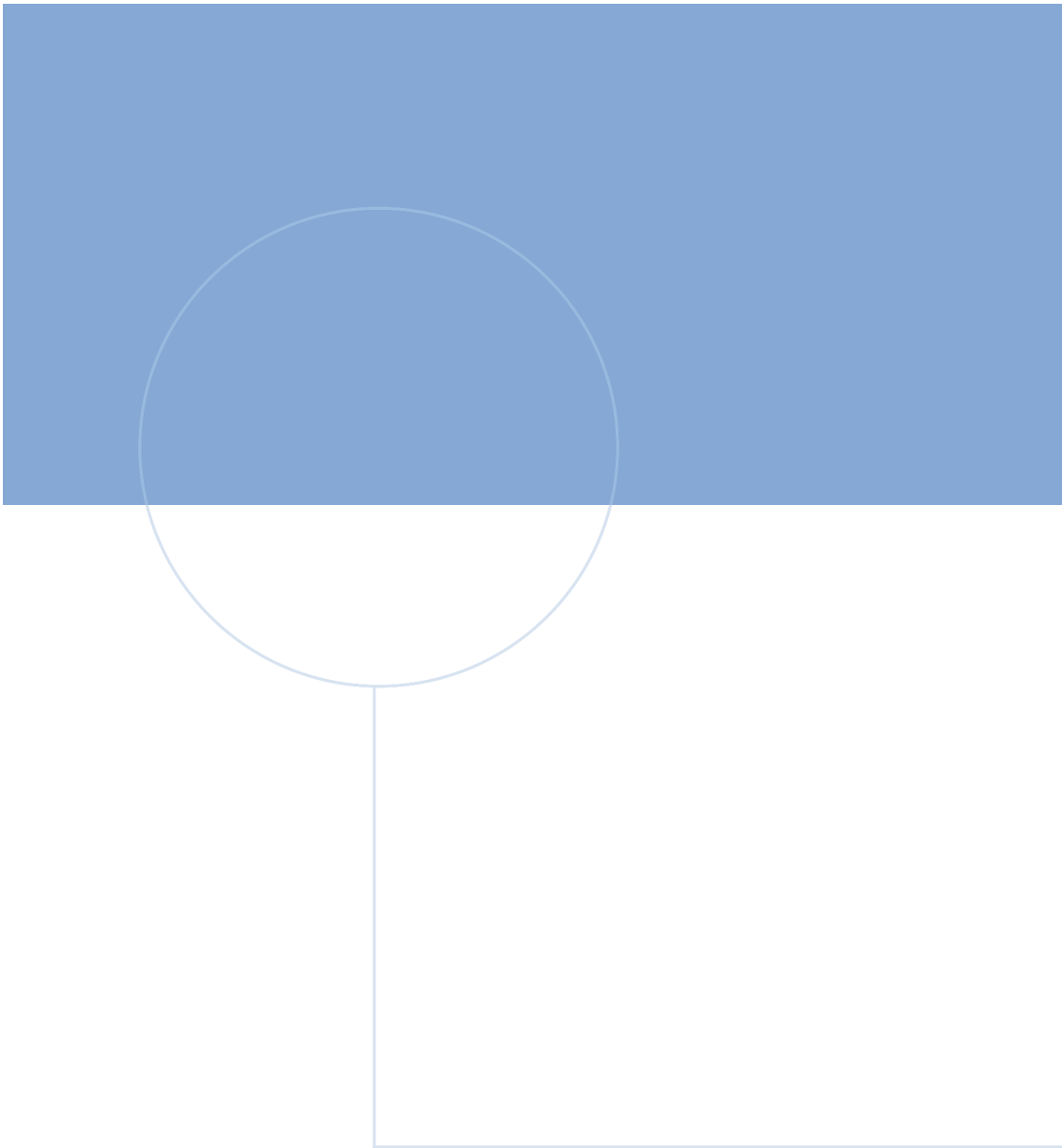

NTNU

Kunnskap for en bedre verden